Pancreatic cancer cells exchange ribosomes through tunneling nanotubes

Authors

Stanislava Martínková, [1] Denisa Jansová, [2] Jana Vorel, [1] Lucie Josefa Lamačová, [1] Petr Daniel, [1] Mário Boďo, [3] Jan Hajer, [4] Andrej Susor, [2] Jan Trnka[1, *]

[1] Department of Biochemistry, Cell and Molecular Biology, Third Faculty of Medicine, Charles University, Prague, Czech Republic

[2] Institute of Animal Physiology and Genetics, The Czech Academy of Sciences, Libechov, Czech Republic

[3] Department of Internal Medicine, Third Faculty of Medicine, Charles University, University Hospital Královské Vinohrady, Prague, Czech Republic

[4] Department of Gastroenterology, Faculty Hospital Bulovka, Prague, Czech Republic

***Correspondence**: jan.trnka@lf3.cuni.cz (J.T.)

Highlights

- PDAC cells derived from tumor biopsy samples form tunneling nanotubes in 2D culture
- Formation of tunneling nanotubes is stimulated by gemcitabine
- 5.8S ribosomal RNA is transferred in PDAC via activated tunneling nanotubes
- Polyadenylated RNA is present in tunneling nanotubes
- Ribosomal components are detected in activated tunneling nanotubes
- PDAC cells exchange assembled ribosomes via tunneling nanotubes
- Ribosomes are transferred via TNTs to recipient cells, incorporated into ribosomes

SUMMARY

Pancreatic ductal adenocarcinoma (PDAC) is recognized as one of the most lethal types of cancer. Tunneling nanotubes (TNTs) are thin membranous intercellular communications, which allow cells to exchange intracellular material and promote cell fitness. We show here that PDAC cells increase the formation of TNTs upon exposure to gemcitabine and that these TNTs contain ribosomal components. In the PANC-1 cell line and in PDAC explants obtained from patient biopsies, we observe polyadenylated RNA and assembled 80S ribosomes within the TNTs, indicating the possibility of an intercellular transfer of translationally active ribosomes. Using cells with labelled small ribosomal subunits (40S), we demonstrate active transport of the ribosomal subunit via TNTs to recipient cells. Our results show that PDAC cells can exchange components of the translational machinery, including mRNA, which may contribute to the resistance to therapy, highlighting the potential of targeting TNT dynamics as a therapeutic approach for PDAC.

KEYWORDS

pancreatic cancer • PDAC • gemcitabine • tunneling nanotubes • 5.8S rRNA • poly(A) mRNA • ribosomal proteins • ribosomes • translation • chemoresistance

INTRODUCTION

Pancreatic ductal adenocarcinoma (PDAC) is one of the deadliest cancers with a poor prognosis with a 5-year overall survival rate of approximately 10%.[1] One of the reasons for the aggressive nature of PDAC is its ability to develop chemoresistance, which ultimately leads to treatment failure and disease progression. Detecting this aggressive cancer in its early stages is crucial for successful treatment outcomes. Gemcitabine monotherapy serves as the established standard of care for patients with worse performance status diagnosed with locally advanced and metastatic pancreatic adenocarcinoma.[2] For patients with good performance status, the FOLFIRINOX (oxaliplatin, irinotecan, leucovorin, fluorouracil) regimen is indicated as

the method of first choice, as it has shown a significant prolongation of median overall survival.[3]

Due to the rapid proliferation, survival mechanisms, epithelial to mesenchymal transition (EMT), invasiveness, and metastasis, cancer cells are presented with unique metabolic requirements. Pancreatic ductal adenocarcinoma cells, growing in hypoxic conditions and encased within dense stroma, adapt through metabolic reprogramming. This adaptation involves a shift to alternative metabolic pathways to fulfil their energy requirements. Predominantly, these cells upregulate aerobic glycolysis, commonly referred to as the Warburg effect, enhance the hexosamine biosynthetic pathway, activate lipid metabolism, and adapt to the deprivation of essential amino acids.[4] The complex adaptations of cancer cells require a high rate of proteosynthesis[5] and pose strict demands on the capacity of the translation machinery.

The upregulation of ribosome biogenesis is an important characteristic of rapidly dividing cells,[6] EMT, metastasis[7] and also of the stem cell phenotype, where the maintenance of long-term replicative plasticity requires a high rate of ribosome synthesis.[8] Dependence on a high rate of ribosome biogenesis has been documented also in cancer stem cells and related to poor disease prognosis.[9] The inhibition of rRNA production has been shown to inhibit tumor growth.[10] An inhibitor of RNA polymerase I exhibited antiproliferative activity in cancer cells and tumor xenografts,[11–13] further supporting the importance of ribosomal biogenesis for cancer cell population.

Tunneling nanotubes (TNTs) are intercellular direct cytoplasmic communication channels that allow cells to transmit signals and cellular components over long distances.[14] Tunneling nanotubes were first observed in rat pheochromocytoma PC12 cells, as well as in human embryonic kidney cells and normal rat kidney cells. These structures typically had a diameter ranging from 50 to 200 nm and could extend several cell diameters in length. Importantly, they did not lie on the substrate.[15] Typically reported intercellular distances are between ten to several hundred μm.[16,17] TNTs can transport mitochondria,[18] ions,[19] organelle-derived vesicles (endosomes, lysosomes), proteins, non-coding RNA.[18,20–22] Recent studies have documented the role of TNTs in the transmission of SARS-CoV-2.[23] In cancer research, TNTs have been observed in glioblastoma patient-derived organoids

transporting mitochondria[24] and in mesenchymal stem cells transferring mitochondria to glioblastoma stem cells via TNTs and enhancing resistance to temozolomide;[25] breast cancer cells transferring mitochondria from immune cells through nanotubes;[26] in prostate cancer, TNTs contribute to the adaptation and treatment resistance through mechanisms involving PI3K/AKT signaling, actin remodeling, and the transport of stress-induced proteins;[27] in bladder cancer TNTs connect heterogeneous cells and facilitate the mitochondrial transfer, leading to increased invasiveness both *in vivo* and *in vitro.*[28] The formation of TNTs can also be induced in a dose-dependent manner by doxorubicin *in vitro* with the resulting drug redistribution via TNTs presenting a new addition on cellular mechanisms of drug efflux and the development of drug resistance in cancers.[29] TNT formation can also be triggered by low serum, hyperglycemic, acidic growth medium[30] and hypoxia.[31] TNTs are also known to play a role in tumor progression, invasiveness and metastasis.[28,32,33]

In this study, we investigated how pancreatic ductal adenocarcinoma cells adapt to increasing doses of the chemotherapeutic agent gemcitabine by augmenting the formation of tunneling nanotubes and by the transfer of ribosomal components and assembled ribosomes between cells.

RESULTS

PDAC biopsy samples develop tunneling nanotubes in 2D cultures

TNTs have previously been detected in cultures of pancreatic cancer cell lines and tumor tissue sample.[29] We used 2D cultures of patient explants from endoscopic biopsies to see whether cultured primary cancer cells can also form these connections. We assessed the formation of tunneling nanotubes in three tissue samples obtained from patients diagnosed with pancreatic ductal adenocarcinoma following endoscopic ultrasound-guided fine needle aspiration biopsy. The patients had not undergone any chemotherapy before the biopsy and their characteristics are summarized in Supplementary Table 1. TNTs were observed in all three cultured tissue samples (Figure 1A, Supplementary Figure S1A). Cells started growing out from the biopsy fragments between 2 to 5 days after plating in a growth medium. All three patients received palliative care. Given that gemcitabine is the most frequently

used first-line treatment for palliative chemotherapy in unresectable PDAC, we investigated whether gemcitabine could affect the formation of TNTs in culture.

Gemcitabine induces TNTs formation in PANC-1 in dose-dependent manner

To determine the optimal dosing regimen, we first estimated the IC50 for gemcitabine in PANC-1 cells to be 1.6 μM (Supplementary Figure S1C). The dense stromal composition and poor vascularization characteristic of PDAC hinder effective drug penetration into the tumor *in vivo*, therefore we used sub-IC50 concentrations for further experiments. We exposed PANC-1 cells to three different sub-IC50 doses of gemcitabine: 0.25 μM, 0.5 μM, and 1 μM for 48 hours and observed a dose-dependent stimulation of the formation of tunneling nanotubes (Figure 1B, 1C), considering only tunneling nanotubes measuring 20 μm or more in length. The observed tunneling nanotubes form above the substrate (Figure 1D), as expected from these structures. This observation suggests that sublethal doses of gemcitabine induce the formation of TNT, potentially influencing the survival and growth ability of pancreatic cancer cells.

Messenger RNA, ribosomal components and assembled translating ribosomes are transported in tunneling nanotubes

Since rapidly dividing cancer cells are highly dependent on proteosynthesis we hypothesized that components of the translation machinery may also be transported through TNTs between PDAC cells. Following a treatment with 0.5 μM gemcitabine for 48 hours to induce the formation of TNTs we detected 5.8S ribosomal RNA (rRNA) within these structures (Figure 2A and Supplementary Figure S2A). This rRNA, which is evolutionarily conserved and a critical component of the large subunit of eukaryotic ribosomes, plays an essential role in protein synthesis. Furthermore, we identified 5.8S rRNA within the TNTs between pancreatic ductal adenocarcinoma cells from a patient's biopsy (Figure 2G, J and Supplementary Figure S2G, J).

We then set out to identify other components of ribosomes in TNTs and found the presence of ribosomal protein S6 and S9 (key components of the 40S subunit) and, ribosomal protein L24 (key component of the 60S subunit) in gemcitabine-activated TNTs in PANC-1 cells (Figure 2B, C, F and Supplementary Figure S2B, C, F)

suggesting the possibility that fully assembled and translationally active ribosomes may be transported between cancer cells via TNTs.

Polyadenylation of RNA contributes to its stabilization and translation. Therefore, we performed *in situ* hybridization with RNA oligo-d(T) probes to visualize polyadenylated RNAs in tunneling nanotubes (Figure 2D and Supplementary Figure S2D). The presence of polyadenylated RNAs complements the detection of ribosomal components and suggests the possibility of transfer of functional, translating ribosomes and mRNA between cells via TNTs.

Functional ribosomes are transferred in TNTs suggesting active translation

To investigate whether the presence of 5.8S ribosomal RNA (rRNA), the both ribosomal subunits and polyadenylated mRNA within tunneling nanotubes supports the hypothesis that functional ribosomes can be transferred between cells, we used the proximity ligation assay (PLA) to detect fully assembled, translation-competent ribosomes.[34,35] We used primary antibodies targeting RPL24 and RPS6, spatially close ribosomal proteins from the 60S and 40S ribosomal subunits, respectively, to generate a multiplexed fluorescent signal through secondary antibodies with hybridization probes that produced single spots indicative of functional 80S ribosomes (Figure 2E and Supplementary figure S2E). According to the crystal structure analysis by Klinge *et al.,*[36] the RPL24 protein forms an intersubunit bridge in the 80S ribosome and interacts with RPS6 protein. Ribosomes identified by the RPL24-RPS6 interaction were distributed within the cytoplasm of PANC-1 cells and in intercellular TNTs. The interaction between RPL24 and RPS6 indicates the formation of the fully assembled 80S ribosomes and ongoing protein synthesis.[34,35] Furthermore, we detected the assembly of ribosomal subunits using the proximity ligation assay for the ribosomal proteins RPS9 and RPL24 ribosomal proteins (Figure 3C and Supplementary Figure S3C). These observations show that tunneling nanotubes contain fully assembled and possibly translationally active ribosomes *en route* between cancer cells.

TNTs are also formed between primary PDAC cancer cells, fibroblasts from biopsy samples and contain assembled ribosomes

To establish that ribosome transport via tunneling nanotubes is not exclusive to the PANC-1 cell line but also occurs in primary human pancreatic tumor cells, we cultured primary human PDAC cells in a 2D culture from thin needle biopsy samples. To ascertain the presence of epithelial tumor cells *in vitro*, we employed a primary antibody against cytokeratin 19, while the detection of stromal cells was confirmed by a primary antibody against vimentin (Figure 2I, L and Supplementary Figure S2I, L). One patient sample (sample 26) was positive for epithelial cells, while the other (sample 24) contained vimentin-positive stromal fibroblasts without any cytokeratin signal. Both patient samples expanded in culture and formed TNTs, which, interestingly, contained significant signals of the two intermediate filament proteins, cytokeratin-19 or vimentin, respectively. Once again, using the RPS6-RPL24 proximity ligation assay we detected assembled ribosomes in these TNTs (Figure 2H, K and Supplementary Figure S2H, K). These data show that functional assembled ribosomes are present in TNTs of primary PDAC cells, as well as in those formed between primary stromal cells.

Functional ribosomes are transported from donor cells to recipient cells via TNTs

To demonstrate that ribosomal proteins are transported from donor to recipient cells via gemcitabine-activated TNTs, inspired by Gallo *et al.,*[37] we generated PANC-1 cells transfected with a mammalian expression vector encoding the human small ribosomal subunit RPS9, C-terminally tagged with HaloTag (donor cells). The donor cells expressed modified RPS9 in the nucleolus, nucleus, and cytoplasm (Supplementary Figure S3E), and a time-lapse video shows the movement of the labelled ribosomal component (Video 1).

Recipient cells were identified either by staining with CellTrace™ Violet stain or by transfection with GFP expressed in the nucleus. After the washing and trypsinization, donor and recipient cells were combined in equal proportions and seeded onto 24-well plates. The mixed cell populations were then treated with gemcitabine for two days to induce the formation of TNTs. Subsequently, the cells were stained with HaloTag TMR Ligand, allowing for the observation of doubly stained cells, in some cases with a TNT connecting a HaloTag positive donor cell with a recipient cell. These observations strongly suggest that tagged RPS9 was exchanged between the

two cell populations through the TNTs (Figure 3A, B and Supplementary Figure S3A, B) and incorporated into ribosomes (Figure 3D and Supplementary Figure S3D).

DISCUSSION

Our results show that ribosomal components 5.8S rRNA, RPS9, RPS6, RPL24, and fully assembled ribosomes together with mRNA are present in TNTs between pancreatic cancer cells and that they are actively transported between the cells. These findings expand the current knowledge about the nature of intracellular material transported in TNTs and show a possible new direction in cancer biology research.

As stated in the Introduction, ribosomal biogenesis has been uncovered as one of key determinants of cancer cell survival, proliferation, adaptation and spread leading to the development of specific inhibitors of rRNA synthesis as possible anticancer agents.[10] Currently used chemotherapeutic agents have also been shown to inhibit rRNA synthesis and ribosome biogenesis, which may contribute to their anticancer effects.[38] Since the intercellular transfer of mitochondria has been proposed as an adaptive mechanism capable of restoring defective mitochondrial function in recipient cells,[39–42] it is perhaps not too far-fetched to see the potential adaptive impact of ribosome transport in cancer cells, which are in many instances dependent on an upregulated rate of ribosome biogenesis and proteosynthesis. The transfer of ribosomes and transcripts via TNTs could be a part of the response to chemotherapy-induced cellular stress, contributing to the survival of recipient cells.

TNTs and chemoresistance

PDAC typically presents irregularly angulated duct-like and glandular structures.[43] These structures are often surrounded by a dense stromal reaction known as desmoplasia, which can contribute to the aggressiveness of PDAC by promoting tumor growth, invasion, and resistance to therapy. Hypovascularity also hinders the delivery of drugs to the tumor, making treatment more challenging.[44] The PDAC surrounding microenvironment is fibroinflammatory and disorganized, composed of extracellular matrix based on collagen, fibronectin, laminin, hyaluronan,[45] cancer-associated fibroblasts,[46] myeloid cells, Treg cells, T cells, B cells, and endothelial cells.[44]

Pancreatic ductal adenocarcinoma has shown resistance to chemotherapy drugs, leading to treatment failure and disease progression. Since 1997, gemcitabine has been a primary monotherapy option for the palliative treatment of PDAC.[47] However, resistance to gemcitabine frequently develops, potentially due to mechanisms such as epithelial-mesenchymal transition, presence of cancer stem cells, dysregulation of the epigenetic factor, overexpression of anti-apoptotic proteins and survival genes, metabolic adaptation complicating treatment and limiting effectiveness.[48,49]

Our results show that sub-IC50 concentrations of gemcitabine induce the formation of TNTs between cancer cells. Since TNTs provide the means of redistributing intracellular components from one cell to another, in the case of mitochondria with a proven adaptive impact,[18,25,26] it is possible to see the induction of TNT formation by gemcitabine as a potential contributor to chemoresistance. The fact, reported in the present study, that ribosomes are also transferred between cells further contributes to this pro-survival and pro-proliferative potential of TNT-mediated transport.

Pancreatic ductal adenocarcinoma is characterized by several key genetic mutations that are frequently observed in the majority of cases. These mutations contribute to the aggressive nature of the disease and affect its progression and response to therapy. The primary genetic mutations associated with PDAC include *KRAS* (present in 94% of cases), *TP53* (64% of cases), *CDKN2A*, and *SMAD4.*[50] An important signaling pathway implicated in the development of PDAC is the PI3K/AKT pathway. This pathway frequently becomes dysregulated in PDAC and leads to the activation of the mammalian target of rapamycin (mTOR) signaling pathway.[51] The mTOR pathway includes two distinct protein complex subunits, mTORC1 and mTORC2, crucial for regulating cell growth, proliferation, metabolism, initiation of translation, and survival.[52] In this context, studies show that downregulation of the mTOR signaling pathway in cancer impairs the translation of specific genes involved in cell proliferation, metabolism and invasion.[53] Activation of the mTORC1 signaling stimulates, among other things, the phosphorylation of the ribosomal protein S6, promoting cell proliferation and cell growth with a negligible effect on overall protein synthesis.[54–56]

The phosphorylation of RPS6 is a significant factor in the initiation and progression of pancreatic cancer[57] and is related to metastasis and poor prognosis in other types of

cancer[58] , which presents a possible therapeutic target.[59] Furthermore, studies have shown that inhibition of mTORC1 decrease the proliferative ability of PDAC cells both *in vitro* and *in vivo.*[51] Importantly, chemosensitivity to gemcitabine was increased when translational initiation was inhibited.[60] The apparent dependence of PDAC cells on S6 phosphorylation may conceivably be another reason for the transfer of ribosomes between cells with different RPS6 kinase activities due to different nutrient status, growth factor signaling cascade activation, cellular stress levels or other factors.

The trafficking of ribosomes and RNA and the associated regulation of translation between cancer cells may be another factor contributing to their resilience and adaptability, highlighting the pro-survival strategies that influence cancer treatment. The mechanisms of ribosomal and RNA transport via TNTs and its regulation, as well as the detailed impacts of transferred ribosomes and RNAs in recipient cells, need to be further explored to expand the possibilities of treating patients with cancer. Since we have observed the formation of TNTs in both stromal cells and cancer cells, a detailed study of the heterotypic exchange of ribosomes within the tumor could provide further insights into the complex relationships between malignant and supporting cells.

METHODS

Experimental model and subject details

Isolation of patients' PDAC samples from EUS-guided FNAB

Patient samples were collected using fine-needle aspiration biopsy under endoscopic ultrasound (EUS-FNAB) control, which is the standard method for diagnosing pancreatic cancer. A mandrel aspiration needle was employed for the biopsy and removed after insertion into the lesion. Subsequently, several passes of the needle through the fixed lesion were performed under a vacuum, induced by a syringe with a fixable plunger position. The aspirate obtained by needle aspiration was transferred into a collection container with a transfer medium and into another container for cytological examination by the pathologist. Patient preparation for the procedure was similar to other therapeutic upper gastrointestinal endoscopies or biopsies of other abdominal organs. Patients arrived fasting, were informed about the purpose of the

examination and its procedures, and provided their consent by signing an informed consent form. Standard analgosedation was used during the examination, and premedication with antibiotics was administered during the biopsy of cystic lesions. Patients were examined lying on their left side, with the possibility of additional position adjustments. Heart rate, blood pressure, and blood oxygen saturation were monitored throughout the procedure. The conclusion of the results, determined by the diagnostic pathologist, was based on the tissue samples examined in our study.

Cultivation of primary PDAC cells from biopsy tissues in 2D culture

Following EUS-FNAB, fresh patient-derived samples were immediately transferred into transfer medium (TM) composed of DMEM/F-12 Ham nutrient mixture, 10% fetal bovine serum (FBS), 1% Penicillin/Streptomycin, and 50 µg/mL Primocin at final concentrations, and transported on ice to the laboratory. Tissues were transferred using a pre-wetted pipette and tweezers onto a sterile glass Petri dish containing drops of wash medium with the same composition as the transfer medium. The tissue underwent five rounds of washing, with each round involving the gradual transfer of the tissue to new drops of wash medium. Subsequently, the tissue samples were minced into smaller fragments measuring 1–2 mm^3 each using a scalpel in a separate drop of wash medium. These tissue fragments were then placed at the center of a 12-well plate, pre-coated with rat tail collagen, and submerged in pre-warmed growth Biojepan culture medium (BCM). The BCM culture medium consisted of DMEM/Nutrient Mixture F-12 Ham, 2% fetal bovine serum, 2 mM GlutaMAX, 1% Penicillin/Streptomycin, 5 µg/mL insulin, 10 ng/mL epidermal growth factor, 0.4 µg/mL hydrocortisone, 10 µM Y-27632, and 50 µg/mL Primocin at final concentrations. The plate was transferred to an incubator set at 37°C and 5% CO_2. The growth BCM medium was refreshed every 2–3 days.

Pancreatic cancer tissue was obtained from patients undergoing tissue biopsies at University Hospital Kralovske Vinohrady in Prague. Written informed consent was obtained from all patients. The study was approved by the Ethics Committee of the University Hospital Kralovske Vinohrady (EK-VP/05/0/2023) and adhered to the Declaration of Helsinki.

PANC-1 cultivation and cell viability assay

PANC-1 cells were seeded at a density of six hundred viable cells per well in a 96-well plate and cultured in 100 µL of DMEM supplemented with 10% fetal bovine

serum (FBS) and 1% Penicillin/Streptomycin (complete DMEM medium) at 37°C and 5% CO_2. For the viability assay and determination of IC50 the medium was replaced after 24 hours of cultivation with a medium supplemented with varying concentrations of gemcitabine. Each experiment was set up in technical triplicates with gemcitabine concentration ranging from 1.0×10^{-8} to 1.0×10^{-4} mol/L. After 3 days of treatment, cell viability was assessed using CellTiter-Glo as per the manufacturer's instructions, and relative luminescence units were measured using the TECAN Infinite M200Pro microplate reader. The measured values of luminescence were obtained from three independent experiments, and the data were recorded for analysis. The dose-response model was created using the *drc* package with a four-parameter log-logistic function and the minimum fixed at 0 and the maximum fixed at the untreated control. The dose-response curve is in Supplementary Figure S1C, and data and R script available at https://github.com/trnkaj/ribosomes.

PANC-1 TNTs activation and counting

The human PANC-1 cell line was cultured as described above. For the dose-response curve of TNT numbers vs. gemcitabine concentration we exposed cells to 0.25 μM, 0.5 μM, and 1 μM of gemcitabine for 2 days. The F-actin in live cells was stained using CellMask Green Actin Tracking Stain to detect TNTs in both the control and gemcitabine-treated groups. TMRM was used for staining mitochondria at a final concentration 100 nM. Hoechst 33342 cell-permeant nuclear counterstain was applied at a final concentration of 5 μg/mL for cell counting purposes. The cells were then incubated with the staining solutions for 30 minutes at 37°C in a 5% CO_2 incubator.

Four random regions of interest (ROIs) were selected, and scanning was performed using a Plan Fluor 4x objective (0.13 NA) in DAPI, FITC and TRITC field modes. Imaging was conducted with a monochrome pco.panda 4.2 camera mounted on the camera port of a Nikon Eclipse Ts2 fluorescence inverted manual microscope. TNTs in both control and treated cells were counted in four independent images. The number of TNTs at each concentration of gemcitabine was normalized to 1×10^4 cells. For nuclear counting and TNT detection, NIS-AR Elements software was used. Measurements were obtained from three independent experiments, and the data were recorded for analysis.

For analyses of ribosomal components, we exposed PANC-1 cells to 0.5 μM gemcitabine for 48 hours prior to microscopy. Patient-derived cells were not exposed to gemcitabine.

Bayesian linear model of dose-dependence

We use a linear model to estimate the dose-dependence of TNT formation on gemcitabine concentration. The model:

$y_i \sim Normal(\mu, \sigma)$

$\mu_i = \alpha + \beta x_i$

$\alpha \sim Normal(0,1)$

$\beta \sim Normal(0,1)$

$\sigma \sim Exponential(1)$

used normalized values of the number of TNTs (*y*) and gemcitabine concentration (*x*) and was estimated using the weakly informative priors with STAN via the *rethinking* package by Richard McElreath. The source data and R code are available at https://github.com/trnkaj/ribosomes

Immunocytochemistry

The PANC-1 cell line was treated for 2 days with 0.5 μM gemcitabine for TNT activation. PDAC primary cells isolated from EUS-FNAB patient samples were grown on a cover glass for immunofluorescence purposes. The samples were fixed in 4% paraformaldehyde in phosphate-buffered saline (DPBS) pH 7.4 for 15 minutes at room temperature (RT). The samples were then washed three times in 1% BSA/DPBS, each lasting 5 minutes, and permeabilized for 20 minutes with 1% BSA/DPBS containing 0.1% Triton X-100 at RT. Afterward, cells were washed three times for 5 minutes each in 1% BSA/DPBS and blocked using a solution of 1% BSA/DPBS to prevent non-specific antibody binding. After 1 hour of blocking, primary antibodies were added and diluted in 1% BSA/DPBS. The cells were then incubated with primary antibodies overnight (O/N) in a humidified chamber at 4°C. The following primary antibodies were used: anti-rRNA antibody (Immunogen: whole 5.8S ribosomal RNA), anti-RPS6 antibody, anti-RPS9 antibody, anti-RPL24 antibody, anti-vimentin antibody, and anti-cytokeratin 19 antibody. Subsequently, the samples

underwent three 10-minute washes, and were then incubated with the relevant Alexa Fluor 488/546/647 conjugated secondary antibody for 2 hours at RT in the dark. Following the incubation, the samples were rinsed three times with 1% BSA/DPBS for 10 minutes each. ActinGreen™ 488 ReadyProbes or ActinRed™ 555 ReadyProbes were used for F-actin staining. Subsequently, the samples underwent another three washes with 1% BSA/DPBS before being mounted in VECTASHIELD® Antifade Mounting Medium with DAPI.

Proximity ligation assay (PLA) of 80S ribosome complex

The PANC-1 cell line with activated TNTs, seeded on cover glass, was fixed for 15 minutes in 4% paraformaldehyde in DPBS and permeabilized for 20 minutes in 0.1% Triton X-100 in DPBS. The PLA Duolink kit blocking solution was then added to the sample. For the three types of PLA experiments, three different combinations of the primary antibody were used. For the first variant, the cells were incubated with primary antibodies rabbit anti-RPL24 (1:100) and mouse anti-RPS6 (1:150) at 4°C O/N. For the second variant, anti-RPL24 (1:100) and mouse anti-RPS9 (1:150) were used. For the third variant, anti-RPL24 (1:100) and Anti-HaloTag® Monoclonal Antibody (1:250) were used. The samples were washed in DPBS and then in Wash Buffer A. They were incubated with 240 μL of reaction mixture (48 μL PLA probe MINUS stock, 48 μL PLA probe PLUS stock and 144 μL DPBS) in a chamber for 1 hour at 37°C. The cells were washed in 1× Wash Buffer A for 6 × 2 minutes, followed by ligation performed in 240 μL of reaction mixture containing 6 μL of ligase, 48 μL of ligation buffer, and 186 μL of molecular H_2O. Samples were incubated in the ligation reaction mixture for 30 minutes at 37°C and then washed 6 × 2 minutes in Wash Buffer A. Next, 240 μL of amplification reaction mixture (3 μL polymerase and 48 μL amplification solution) was added to each sample before incubation at 37°C for 100 minutes. The samples were washed in 500 μL of Wash Buffer B for 3 × 5 minutes and 1 × 2 minutes in 0.01× Wash Buffer B. ActinRed™ 555 ReadyProbes was used for F-actin staining according to the manufacturer's instructions. Finally, the samples were mounted using VECTASHIELD® Mounting Medium with DAPI. For the PLA assays, three combinations were used: one detecting the interaction between RPL24 and RPS6, the second detecting the interaction between RPL24 and RPS9, and the third aimed at detecting the interaction between RPL24 and RPS9 expressed from the pHTC-hsRPS9-HaloTag® CMV-neo vector.

RNA fluorescent in situ hybridization (FISH) – PolyA

Cells with activated TNTs, seeded on cover glass, were fixed for 15 minutes in 4% paraformaldehyde and permeabilized with 1% Triton X-100 in DPBS. The samples were washed in 900 µL of 1× wash buffer A and incubated O/N at 42°C in a hybridization buffer with 75 nM oligo-d(T) probe and CalFluorRed635. The samples were then washed twice in wash buffer A and twice in 2× SSC. ActinGreen™ 488 ReadyProbes was used for F-actin staining according to the manufacturer's instructions. Finally, the samples were mounted in VectaShield medium with DAPI.

Cloning

For the cloning strategy, total RNA was isolated from MCF-7 breast cancer cells (RRID: CVCL_0031) using the RNeasy Kit according to the manufacturer's instructions. Two micrograms of total RNA were reverse transcribed by oligo$(dT)_{18}$ in a 20 µL reaction using the Maxima H Minus First Strand cDNA Synthesis Kit following a modified protocol: 50°C for 30 minutes followed by 55°C for 30 minutes. Then, cDNA equivalent to 20 ng of mRNA served as a nested PCR template in a total volume of 50 µL. The first PCR was done with the CLO_hsRPS9_FOR and CLO_hsRPS9_REV pair of primers specific to the 5' and 3' untranslated regions of human RPS9. Primers for the second PCR, CLO_hsRPS9Eco_FOR and CLO_hsRPS9Xho_REV were situated to encompass RPS9 open reading frame except the stop codon. Both PCR reactions ran for 35 cycles with Q5 high-fidelity polymerase under similar conditions: initial denaturation at 95°C for 2 minutes, denaturation at 95°C for 20 seconds, annealing 63.8°C for 20 seconds, extension at 72°C for 40 seconds and final extension at 72°C for 3 minutes. The product of the second PCR was cloned via *Eco*RI and *Xho*I sites in frame with the C-terminal Halo® Tag to generate pHTC-hsRPS9-HaloTag® CMV-neo vector (Supplementary figure S4). The insert was sequenced using CMV universal sequencing primer CMV_FOR.

Transfection

The PANC-1 cell line was cultured in complete DMEM medium at 37°C with 5% CO_2. Upon reaching 70% confluence on a 24-well plate, the cells were transfected with the pHTC-hsRPS9-HaloTag® CMV-neo vector using Lipofectamine™ 3000 Transfection Reagent (donor cells) according to the manufacturer's instructions. Two days after transfection, the medium was replaced with fresh complete DMEM.

Two variants of PANC-1 recipient cells were used: one with the nucleus stained using CellLight™ Nucleus-GFP, BacMam 2.0, and the other with the entire cell stained with the covalent CellTrace™ Violet Cell Proliferation Kit, both following the manufacturer's instructions.

The wells containing donor and recipient cells were washed three times with prewarmed DPBS at 37°C prior to trypsinization, before seeding them for the co-culturing experiment. After three minutes of enzymatic detachment treatment and trypsin inhibition, the cells were centrifuged at 350 x g for 5 minutes. The supernatant was discarded, and the cells were washed with prewarmed complete DMEM medium and centrifuged a second time. The supernatant was discarded, and the cells were resuspended in complete DMEM medium. Donor and recipient cells were then co-seeded onto a 24-well plate. One day post-seeding, the cells were treated with 0.5 µM gemcitabine to activate TNTs for two days. For live cell microscopy, the cells were stained with HaloTag® TMR Ligand to detect expressed RPS9 from the vector. Images were captured on a Nikon Eclipse Ts2 fluorescence inverted manual microscope. Live cell video of transport of HaloTag RPS9 was recorded using a Leica Stellaris 8 confocal microscope.

Fluorescence and confocal microscopy

For scanning fluorescently labeled samples, a Leica Stellaris 8 confocal microscope (indicated by * in the respective images) and a Nikon Eclipse Ts2 fluorescence inverted manual microscope (indicated by # in the respective images) were used. An inverted routine fluorescence microscope (Nikon Eclipse Ts2) was equipped with Plan Fluor 4x objective (0.13 NA), Plan Fluor 10x objective (0.30 NA), S Plan Fluor ELWD 20x objective (0.45 NA) and S Plan Fluor ELWD 40x objective (0.60 NA). Next, an inverted confocal microscope (Leica Stellaris 8) with a Glycine 40x objective (1.25 NA) was used for sample visualization. The inverted microscope, equipped with a controlled chamber system (Temp Controller 2000–2, Pecon and a CO_2 Controller, Pecon), was used for time-lapse recordings. The images were processed using NIS-Elements Advanced Research, Leica Application Suite (LAS X), and ImageJ/FIJI.

Material table

Antibodies	Source	Code
rRNA Monoclonal Antibody (Y10b)	Thermo Fisher	MA1-16628
RPL24 Polyclonal Antibody	Invitrogen™, Thermo Fisher	PA5-62450
Ribosomal Protein S6 Antibody (C-8)	Santa cruz biotechnology	sc-74459
Anti-HaloTag® Monoclonal Antibody	Promega	G9211
Anti-Vimentin antibody	Abcam	ab92547
Anti-Cytokeratin 19 antibody	Abcam	ab9221
Donkey anti-Rabbit IgG (H+L) Highly Cross-Adsorbed Secondary Antibody, Alexa Fluor™ 488	Invitrogen™, Thermo Fisher	A-21206
Goat anti-Mouse IgG (H+L) Cross-Adsorbed Secondary Antibody, Alexa Fluor™ 546	Invitrogen™, Thermo Fisher	A-11003
Goat anti-Rabbit IgG (H+L) Highly Cross-Adsorbed Secondary Antibody, Alexa Fluor™ 647	Invitrogen™, Thermo Fisher	A-21245
Goat anti-Mouse IgG (H+L) Highly Cross-Adsorbed Secondary Antibody, Alexa Fluor™ Plus 647	Invitrogen™, Thermo Fisher	A32728
Chemicals	**Source**	**Code**
DMEM/Nutrient Mixture F-12 Ham	Sigma-Aldrich	D6434
DMEM, low glucose, pyruvate	Gibco™ Thermo Fisher	31885-023
DPBS, no calcium, no magnesium	Gibco™ Thermo Fisher	14190144
Fetal Bovine Serum, qualified, Brazil	Gibco™ Thermo Fisher	10270106
GlutaMAX™ Supplement	Gibco™ Thermo Fisher	35050061
Penicillin-Streptomycin	Sigma-Aldrich	P4333
Primocin® Antimicrobial agent for primary cells	InvivoGen	Ant-pm-1
Insulin, human recombinant, zinc solution	Gibco™ Thermo Fisher	12585014
Human EGF Recombinant Protein	Gibco™ Thermo Fisher	PHG0311
Hydrocortisone, 98%, Thermo Scientific Chemicals	Thermo Scientific Chemicals	A16292.03
Y-27632 (dihydrochloride)	MedChemExpres s	129830-38-2
Trypsin-EDTA (0.5%), no phenol red	Gibco™ Thermo Fisher	15400054
Collagen I, rat tail	Gibco™ Thermo Fisher	A1048301
Acetic acid	Sigma-Aldrich	V800019

Gemcitabine hydrochloride, 98%	Thermo Scientific Chemicals	461060010
Paraformaldehyde	Sigma-Aldrich	158127-100G
Triton™ X-100	Sigma-Aldrich	T8787
Bovine Serum Albumin	Sigma-Aldrich	A7030-100G
Nuclease-Free Water (not DEPC-Treated)	Invitrogen™ Thermo Fisher	AM9937
Stellaris® RNA FISH Hybridization Buffer	Biosearch Technologies	SMF-HB1-10
Stellaris® RNA FISH Wash Buffer A	Biosearch Technologies	SMF-WA1-60
Stellaris® RNA FISH Wash Buffer B	Biosearch Technologies	SMF-WB1-20
SSC Buffer 20× Concentrate	Sigma-Aldrich	S6639
Hoechst 33342	Invitrogen™ Thermo Fisher	H1399
Vectashield Vibrance® Antifade Mounting Medium with DAPI	Vector Laboratories	H-1800
CellMask™ Green Actin Tracking Stain	Invitrogen™ Thermo Fisher	A57243
ActinGreen™ 488 ReadyProbes™ Reagent (AlexaFluor™ 488 phalloidin)	Invitrogen™ Thermo Fisher	R37110
ActinRed™ 555 ReadyProbes™ Reagent (Rhodamine phalloidin)	Invitrogen™ Thermo Fisher	R37112
HaloTag® TMR Ligand	Promega	G8251
CellLight™ Nucleus-GFP, BacMam 2.0	Invitrogen™ Thermo Fisher	C10602
CellTrace™ Violet Cell Proliferation Kit, for flow cytometry	Invitrogen™ Thermo Fisher	C34571
Q5® High-Fidelity DNA Polymerase	NEB, Ipswich	M0491S
Assays and Kits	**Source**	**Code**
CellTiter-Glo Luminescent Cell Viability Assay	Promega	G7571
Duolink® In Situ PLA® Probe Anti-Rabbit MINUS	Sigma-Aldrich	DUO92005
Duolink® In Situ PLA® Probe Anti-Mouse PLUS	Sigma-Aldrich	DUO92001
Duolink® In Situ Probemaker MINUS	Sigma-Aldrich	DUO92010
Duolink® In Situ Detection Reagents Green	Sigma-Aldrich	DUO92014
Duolink® In Situ Wash Buffers, Fluorescence	Sigma-Aldrich	DUO 82049
Lipofectamine™ Transfection Reagent	Invitrogen™ Thermo Fisher	18324012
RNeasy Mini Kit (50)	Qiagen	74104

Maxima H Minus First Strand cDNA Synthesis Kit	Thermo Scientific™ Thermo Fisher	K1652
Opti-MEM Reduced Serum Medium	Gibco™ Thermo Fisher	31985-062
Oligonucleotides	**Source**	**Code**
Polydt proba cy5- Sequence: NTTTTTTTTTTTTTTTTTTTT	biotech genery costume probe	1351P3
CLO_hsRPS9_FOR (5'-GGTGGTTTGCTTAGGCGCAGACG-3')	first PCR custome primer, Sigma-Aldrich	VC00021N
CLO_hsRPS9_REV (5'-GAGACAATCCAGCAGCCCAGGAG-3')	first PCR custome primer, Sigma-Aldrich	VC00021N
CLO_hsRPS9Eco_FOR (5'-ATATAAT*GAATTC*ACCATGCCAGTGGCCCGGAGCTG-3')	cloning second PCR custom primer, Sigma-Aldrich	VC00021N
CLO_hsRPS9Xho_REV (5'-AATAGTA*CTCGAG*ATCCTCCTCCTCGTCGTCTCC-3')	cloning second PCR custom primer, Sigma-Aldrich	VC00021N
Biological samples and experimental cell line	**Source**	**Code**
Human patient samples	University Hospital Kralovske Vinohrady, Prague	N/A
PANC-1 Cell Line	Sigma-Aldrich	87092802-1VL
Recombinant DNA	**Source**	**Code**
pHTC HaloTag® CMV-neo-Vector	Promega	G7711
pHTC-hsRPS9-HaloTag® CMV-neo	This paper	N/A
Culture Plastics and Cover glass	**Source**	**Code**
Nunc™ Cell-Culture Treated Multidishes	Thermo Scientific™ Thermo Fisher	150628
Nunc™ Cell-Culture Treated Multidishes	Thermo Scientific™ Thermo Fisher	142475
Nunc™ MicroWell™ 96-Well, Nunclon Delta-Treated	Thermo Scientific™ Thermo Fisher	136101
Round cover glasses, Menzel Gläser 12 mm Ø, # 1.5	Epredia™ Menzel™, Fisher Scientific	MENZCB00120RAC20
Laboratory instruments	**Source**	**Code**
Infinite M200Pro microplate reader	TECAN	equipment

Nikon Eclipse Ts2 fluorescence microscope	Nikon	equipment
Leica confocal microscope Stellaris 8	Leica	equipment
Software	**Source**	**Code**
NIS-elements	Nikon	AR 5.20.00
R version 4.4.0 (2024-04-24)	The R Project for Statistical Computing	https://www.r-project.org/
Leica Application Suite X (LAS X)	Leica	LAS X 4.7.0.28176
Fiji ImageJ	Wayne Rusband; National Institute of Health	https://imagej.net/software/fiji/

ACKNOWLEDGMENTS

This work was supported by funding by Institutional Research Concept RV067985904, the Czech Science Foundation [22-27301S], CARDIA, project EXCELES LX22NPO5104 funded by Next Generation EU, and by grant from Charles University GAUK 108624.

AUTHOR CONTRIBUTIONS

S.M., J.T. and A.S. designed experiments. S.M., J.T., D.J., J.V., L.J.L., P.D. and A.S. analyzed data from experiments. S.M. cultivated primary patient PDAC cells from biopsy, performed PANC-1 cell viability assay, immunocytochemistry, transfection, and fluorescence microscopy scanning of images. D.J. performed and analyzed PLA assay, FISH and confocal scanning of images. J.V. and L.J.L. performed TNT activation and TNT analysis. P.D. performed cloning and verification of the HaloTag construct. M.B. and J.H. performed biopsies of PDAC patients and collected clinical data. S.M. and J.T. wrote the manuscript with input from all co-authors, all co-authors read and edited the final manuscript.

DECLARATION OF INTEREST

The authors declare no competing interests.

RESOURCE AVAILABILITY

Lead contact

Further information and requests for resources and reagents should be directed to and will be fulfilled by the lead contact, Jan Trnka (jan.trnka@lf3.cuni.cz)

Data and code availability

- All data reported in this paper is available at https://github.com/trnkaj/ribosomes.
- This paper reports original code available at https://github.com/trnkaj/ribosomes.
- Any additional information required to reanalyze the data reported in this paper is available from the lead contact upon request.

REFERENCES

1. Grossberg, A.J., Chu, L.C., Deig, C.R., Fishman, E.K., Hwang, W.L., Maitra, A., Marks, D.L., Mehta, A., Nabavizadeh, N., Simeone, D.M., et al. (2020). Multidisciplinary standards of care and recent progress in pancreatic ductal adenocarcinoma. CA Cancer J Clin *70*, 375–403. https://doi.org/10.3322/CAAC.21626.
2. Burris, H.A., Moore, M.J., Andersen, J., Green, M.R., Rothenberg, M.L., Modiano, M.R., Cripps, M.C., Portenoy, R.K., Storniolo, A.M., Tarassoff, P., et al. (2016). Improvements in survival and clinical benefit with gemcitabine as first-line therapy for patients with advanced pancreas cancer: a randomized trial. J Clin Oncol *15*, 2403–2413. https://doi.org/10.1200/JCO.1997.15.6.2403.
3. Conroy, T., Desseigne, F., Ychou, M., Bouché, O., Guimbaud, R., Bécouarn, Y., Adenis, A., Raoul, J.-L., Gourgou-Bourgade, S., de la Fouchardière, C., et al. (2011). FOLFIRINOX versus Gemcitabine for Metastatic Pancreatic Cancer. N Engl J Med *364*, 1817–1825. https://doi.org/ 10.1056/NEJMoa1011923.
4. Zuzčák, M., and Trnka, J. (2022). Cellular metabolism in pancreatic cancer as a tool for prognosis and treatment (Review). Int J Oncol *61*. https://doi.org/10.3892/IJO.2022.5383.
5. Dolfi, S.C., Li, L., Chan, -Ying, Qiu, J., Tedeschi, P.M., Bertino, J.R., Hirshfield, K.M., Oltvai, Z.N., and Vazquez, A. (2013). The metabolic demands of cancer cells are coupled to their size and protein synthesis rates. Cancer & Metabolism *1*, 1–13. https://doi.org/10.1186/2049-3002-1-20.
6. Donati, G., Montanaro, L., and Derenzini, M. (2012). Ribosome biogenesis and control of cell proliferation: p53 is not alone. Cancer Res *72*, 1602–1607. https://doi.org/10.1158/0008-5472.CAN-11-3992.
7. Prakash, V., Carson, B.B., Feenstra, J.M., Dass, R.A., Sekyrova, P., Hoshino, A., Petersen, J., Guo, Y., Parks, M.M., Kurylo, C.M., et al. (2019). Ribosome biogenesis during cell cycle arrest fuels EMT in development and disease. Nat Commun *10*. https://doi.org/10.1038/S41467-019-10100-8.
8. Flach, J., Bakker, S.T., Mohrin, M., Conroy, P.C., Pietras, E.M., Reynaud, D., Alvarez, S., Diolaiti, M.E., Ugarte, F., Forsberg, E.C., et al. (2014). Replication stress is a potent driver of functional decline in ageing haematopoietic stem cells. Nature *512*, 198–202. https://doi.org/10.1038/NATURE13619.
9. Morral, C., Stanisavljevic, J., Hernando-Momblona, X., Mereu, E., Álvarez-Varela, A., Cortina, C., Stork, D., Slebe, F., Turon, G., Whissell, G., et al. (2020). Zonation of Ribosomal DNA Transcription Defines a Stem Cell Hierarchy in Colorectal Cancer. Cell Stem Cell *26*, 845-861.e12. https://doi.org/10.1016/J.STEM.2020.04.012.
10. Bywater, M.J., Poortinga, G., Sanij, E., Hein, N., Peck, A., Cullinane, C., Wall, M., Cluse, L., Drygin, D., Anderes, K., et al. (2012). Inhibition of RNA polymerase I as a therapeutic strategy to promote cancer-specific activation of p53. Cancer Cell *22*, 51–65. https://doi.org/10.1016/J.CCR.2012.05.019.
11. Cornelison, R., Dobbin, Z.C., Katre, A.A., Jeong, D.H., Zhang, Y., Chen, D., Petrova, Y., Llaneza, D.C., Steg, A.D., Parsons, L., et al. (2017). Targeting RNA-Polymerase I in Both Chemosensitive and Chemoresistant Populations in Epithelial Ovarian Cancer. Clin Cancer Res *23*, 6529–6540. https://doi.org/10.1158/1078-0432.CCR-17-0282.

12. Negi, S.S., and Brown, P. (2015). rRNA synthesis inhibitor, CX-5461, activates ATM/ATR pathway in acute lymphoblastic leukemia, arrests cells in G2 phase and induces apoptosis. Oncotarget *6*, 18094–18104. https://doi.org/10.18632/ONCOTARGET.4093.
13. Yu, P., Qu, N., Zhu, R., Hu, J., Han, P., Wu, J., Tan, L., Gan, H., He, C., Fang, C., et al. (2023). TERT accelerates BRAF mutant-induced thyroid cancer dedifferentiation and progression by regulating ribosome biogenesis. Sci Adv *9*. https://doi.org/10.1126/SCIADV.ADG7125.
14. Ariazi, J., Benowitz, A., De Biasi, V., Den Boer, M.L., Cherqui, S., Cui, H., Douillet, N., Eugenin, E.A., Favre, D., Goodman, S., et al. (2017). Tunneling Nanotubes and Gap Junctions-Their Role in Long-Range Intercellular Communication during Development, Health, and Disease Conditions. Front Mol Neurosci *10*. https://doi.org/10.3389/FNMOL.2017.00333.
15. Rustom, A., Saffrich, R., Markovic, I., Walther, P., and Gerdes, H.H. (2004). Nanotubular highways for intercellular organelle transport. Science *303*, 1007–1010. https://doi.org/10.1126/SCIENCE.1093133.
16. Austefjord, M.W., Gerdes, H.H., and Wang, X. (2014). Tunneling nanotubes: Diversity in morphology and structure. Commun Integr Biol *7*, e27934. https://doi.org/10.4161/CIB.27934.
17. Zurzolo, C. (2021). Tunneling nanotubes: Reshaping connectivity. Curr Opin Cell Biol *71*, 139–147. https://doi.org/10.1016/J.CEB.2021.03.003.
18. Hekmatshoar, Y., Nakhle, J., Galloni, M., and Vignais, M.L. (2018). The role of metabolism and tunneling nanotube-mediated intercellular mitochondria exchange in cancer drug resistance. Biochemical Journal *475*, 2305–2328. https://doi.org/10.1042/BCJ20170712.
19. Smith, I.F., Shuai, J., and Parker, I. (2011). Active Generation and Propagation of Ca2+ Signals within Tunneling Membrane Nanotubes. Biophys J *100*, L37–L39. https://doi.org/10.1016/J.BPJ.2011.03.007.
20. Abounit, S., Delage, E., and Zurzolo, C. (2015). Identification and characterization of tunneling nanotubes for intercellular trafficking. Curr Protoc Cell Biol *2015*, 12.10.1-12.10.21. https://doi.org/10.1002/0471143030.cb1210s67.
21. Murray, L.M.A., and Krasnodembskaya, A.D. (2019). Concise Review: Intercellular Communication Via Organelle Transfer in the Biology and Therapeutic Applications of Stem Cells. Stem Cells *37*, 14–25. https://doi.org/10.1002/STEM.2922.
22. Haimovich, G., Dasgupta, S., and Gerst, J.E. (2021). RNA transfer through tunneling nanotubes. Biochem Soc Trans *49*, 145–160. https://doi.org/10.1042/BST20200113.
23. Pepe, A., Pietropaoli, S., Vos, M., Barba-Spaeth, G., and Zurzolo, C. (2022). Tunneling nanotubes provide a route for SARS-CoV-2 spreading. Sci Adv *8*, 171. https://doi.org/ 10.1126/sciadv.abo0171.
24. Pinto, G., Saenz-De-Santa-Maria, I., Chastagner, P., Perthame, E., Delmas, C., Toulas, C., Moyal-Jonathan-Cohen, E., Brou, C., and Zurzolo, C. (2021). Patient-derived glioblastoma stem cells transfer mitochondria through tunneling nanotubes in tumor organoids. Biochem J *478*, 21–39. https://doi.org/10.1042/BCJ20200710.
25. Nakhle, J., Khattar, K., Özkan, T., Boughlita, A., Abba Moussa, D., Darlix, A., Lorcy, F., Rigau, V., Bauchet, L., Gerbal-Chaloin, S., et al. (2023). Mitochondria Transfer from Mesenchymal Stem Cells Confers Chemoresistance to Glioblastoma

Stem Cells through Metabolic Rewiring. Cancer Res Commun *3*, 1041–1056. https://doi.org/10.1158/2767-9764.CRC-23-0144.
26. Saha, T., Dash, C., Jayabalan, R., Khiste, S., Kulkarni, A., Kurmi, K., Mondal, J., Majumder, P.K., Bardia, A., Jang, H.L., et al. (2021). Intercellular nanotubes mediate mitochondrial trafficking between cancer and immune cells. Nature Nanotechnol *17*, 98–106. https://doi.org/10.1038/s41565-021-01000-4.
27. Kretschmer, A., Zhang, F., Somasekharan, S.P., Tse, C., Leachman, L., Gleave, A., Li, B., Asmaro, I., Huang, T., Kotula, L., et al. (2019). Stress-induced tunneling nanotubes support treatment adaptation in prostate cancer. Sci Rep *9*, 1–13. https://doi.org/10.1038/s41598-019-44346-5.
28. Lu, J., Zheng, X., Li, F., Yu, Y., Chen, Z., Liu, Z., Wang, Z., Xu, H., and Yang, W. (2017). Tunneling nanotubes promote intercellular mitochondria transfer followed by increased invasiveness in bladder cancer cells. Oncotarget *8*, 15539–15552. https://doi.org/10.18632/ONCOTARGET.14695.
29. Desir, S., O'hare, P., Vogel, R.I., Sperduto, W., Sarkari, A., Dickson, E.L., Wong, P., Nelson, A.C., Fong, Y., Steer, C.J., et al. (2018). Chemotherapy-Induced Tunneling Nanotubes Mediate Intercellular Drug Efflux in Pancreatic Cancer. Sci Rep *8*, 9484. https://doi.org/10.1038/s41598-018-27649-x.
30. Lou, E., Fujisawa, S., Morozov, A., Barlas, A., Romin, Y., Dogan, Y., Gholami, S., Moreira, A.L., Manova-Todorova, K., and Moore, M.A.S. (2012). Tunneling Nanotubes Provide a Unique Conduit for Intercellular Transfer of Cellular Contents in Human Malignant Pleural Mesothelioma. PLoS One *7*, e33093. https://doi.org/10.1371/JOURNAL.PONE.0033093.
31. Desir, S., Dickson, E.L., Vogel, R.I., Thayanithy, V., Wong, P., Teoh, D., Geller, M.A., Steer, C.J., Subramanian, S., Lou, E., et al. (2016). Tunneling nanotube formation is stimulated by hypoxia in ovarian cancer cells. Oncotarget *7*, 43150–43161. https://doi.org/10.18632/ONCOTARGET.9504.
32. Pinto, G., Brou, C., and Zurzolo, C. (2020). Tunneling Nanotubes: The Fuel of Tumor Progression? Trends Cancer *6*, 874–888. 10.1016/j.trecan.2020.04.012.
33. Hanna, S.J., McCoy-Simandle, K., Leung, E., Genna, A., Condeelis, J., and Cox, D. (2019). Tunneling nanotubes, a novel mode of tumor cell–macrophage communication in tumor cell invasion. J Cell Sci *132*, jcs223321. https://doi.org/10.1242/jcs.223321.
34. Jansova, D., Tetkova, A., Koncicka, M., Kubelka, M., and Susor, A. (2018). Localization of RNA and translation in the mammalian oocyte and embryo. PLoS One *13*, e0192544. https://doi.org/10.1371/JOURNAL.PONE.0192544.
35. Cheng, S., Altmeppen, G., So, C., Welp, L.M., Penir, S., Ruhwedel, T., Menelaou, K., Harasimov, K., Stützer, A., Blayney, M., et al. (2022). Mammalian oocytes store mRNAs in a mitochondria-associated membraneless compartment. Science *378*, eabq4835. https://doi.org/10.1126/science.abq4835.
36. Klinge, S., Voigts-Hoffmann, F., Leibundgut, M., and Ban, N. (2012). Atomic structures of the eukaryotic ribosome. Trends Biochem Sci *37*, 189–198. https://doi.org/10.1016/j.tibs.2012.02.007
37. Gallo, S., Beugnet, A., and Biffo, S. (2011). Tagging of functional ribosomes in living cells by HaloTag® technology. In Vitro Cell Dev Biol Anim *47*, 132–138. https://doi.org/10.1007/S11626-010-9370-7.
38. Burger, K., Mühl, B., Harasim, T., Rohrmoser, M., Malamoussi, A., Orban, M., Kellner, M., Gruber-Eber, A., Kremmer, E., Hölzel, M., et al. (2010).

Chemotherapeutic drugs inhibit ribosome biogenesis at various levels. J Biol Chem *285*, 12416–12425. https://doi.org/10.1074/JBC.M109.074211.
39. Spees, J.L., Olson, S.D., Whitney, M.J., and Prockop, D.J. (2006). Mitochondrial transfer between cells can rescue aerobic respiration. Proc Natl Acad Sci U S A *103*, 1283–1288. https://doi.org/10.1073/PNAS.0510511103.
40. Cho, Y.M., Kim, J.H., Kim, M., Park, S.J., Koh, S.H., Ahn, H.S., Kang, G.H., Lee, J. Bin, Park, K.S., and Lee, H.K. (2012). Mesenchymal stem cells transfer mitochondria to the cells with virtually no mitochondrial function but not with pathogenic mtDNA mutations. PLoS One *7*, e32778. https://doi.org/10.1371/JOURNAL.PONE.0032778.
41. Tan, A.S., Baty, J.W., Dong, L.F., Bezawork-Geleta, A., Endaya, B., Goodwin, J., Bajzikova, M., Kovarova, J., Peterka, M., Yan, B., et al. (2015). Mitochondrial genome acquisition restores respiratory function and tumorigenic potential of cancer cells without mitochondrial DNA. Cell Metab *21*, 81–94. https://doi.org/10.1016/J.CMET.2014.12.003.
42. Ippolito, L., Morandi, A., Taddei, M.L., Parri, M., Comito, G., Iscaro, A., Raspollini, M.R., Magherini, F., Rapizzi, E., Masquelier, J., et al. (2019). Cancer-associated fibroblasts promote prostate cancer malignancy via metabolic rewiring and mitochondrial transfer. Oncogene *38*, 5339–5355. https://doi.org/10.1038/S41388-019-0805-7.
43. Luchini, C., Grillo, F., Fassan, M., Vanoli, A., Capelli, P., Paolino, G., Ingravallo, G., Renzulli, G., Doglioni, C., D'Amuri, A., et al. (2020). Malignant epithelial/exocrine tumors of the pancreas. Pathologica 112, 210–226. https://doi.org/10.32074/1591-951X-167.
44. Sherman, M.H., and Beatty, G.L. (2023). Tumor Microenvironment in Pancreatic Cancer Pathogenesis and Therapeutic Resistance. Annu Rev Pathol *18*, 123–148. https://doi.org/ 10.1146/annurev-pathmechdis-031621-024600.
45. Whatcott, C.J., Han, H., Posner, R.G., Hostetter, G., and Von Hoff, D.D. (2011). Targeting the tumor microenvironment in cancer: why hyaluronidase deserves a second look. Cancer Discov *1*, 291–296. https://doi.org/10.1158/2159-8290.CD-11-0136.
46. Brumskill, S., Barrera, L.N., Calcraft, P., Phillips, C., and Costello, E. (2023). Inclusion of cancer-associated fibroblasts in drug screening assays to evaluate pancreatic cancer resistance to therapeutic drugs. J Physiol Biochem *79*, 223–234. https://doi.org/10.1007/s13105-021-00857-2.
47. Riedl, J.M., Posch, F., Horvath, L., Gantschnigg, A., Renneberg, F., Schwarzenbacher, E., Moik, F., Barth, D.A., Rossmann, C.H., Stotz, M., et al. (2021). Gemcitabine/nab-Paclitaxel versus FOLFIRINOX for palliative first-line treatment of advanced pancreatic cancer: A propensity score analysis. Eur J Cancer *151*, 3–13. https://doi.org/10.1016/j.ejca.2021.03.040.
48. Hekmatshoar, Y., Nakhle, J., Galloni, M., and Vignais, M.L. (2018). The role of metabolism and tunneling nanotube-mediated intercellular mitochondria exchange in cancer drug resistance. Biochem J *31*, 2305–2328. https://doi.org/10.1042/BCJ20170712.
49. Ashrafizadeh, M., Luo, K., Zhang, W., Reza Aref, A., and Zhang, X. (2024). Acquired and intrinsic gemcitabine resistance in pancreatic cancer therapy: Environmental factors, molecular profile and drug/nanotherapeutic approaches. Environ Res *240*, 117443. https://doi.org/10.1016/J.ENVRES.2023.117443.

50. Waters, A.M., and Der, C.J. (2018). KRAS: The Critical Driver and Therapeutic Target for Pancreatic Cancer. Cold Spring Harb Perspect Med *8*, a031435. https://doi.org/ 10.1101/cshperspect.a031435.
51. Awasthi, N., Yen, P.L., Schwarz, M.A., and Schwarz, R.E. (2012). The efficacy of a novel, dual PI3K/mTOR inhibitor NVP-BEZ235 to enhance chemotherapy and antiangiogenic response in pancreatic cancer. J Cell Biochem *113*, 784–791. https://doi.org/10.1002/JCB.23405.
52. Danesh Pazhooh, R., Rahnamay Farnood, P., Asemi, Z., Mirsafaei, L., Yousefi, B., and Mirzaei, H. (2021). mTOR pathway and DNA damage response: A therapeutic strategy in cancer therapy. DNA Repair (Amst) *104*, 103142. https://doi.org/10.1016/J.DNAREP.2021.103142.
53. Hsieh, A.C., Liu, Y., Edlind, M.P., Ingolia, N.T., Janes, M.R., Sher, A., Shi, E.Y., Stumpf, C.R., Christensen, C., Bonham, M.J., et al. (2012). The translational landscape of mTOR signalling steers cancer initiation and metastasis. Nature *485*, 55. https://doi.org/10.1038/NATURE10912.
54. Ruvinsky, I., Sharon, N., Lerer, T., Cohen, H., Stolovich-Rain, M., Nir, T., Dor, Y., Zisman, P., and Meyuhas, O. (2005). Ribosomal protein S6 phosphorylation is a determinant of cell size and glucose homeostasis. Genes Dev *19*, 2199–2211. https://doi.org/10.1101/GAD.351605.
55. Meyuhas, O. (2015). Ribosomal Protein S6 Phosphorylation: Four Decades of Research. Int Rev Cell Mol Biol *320*, 41–73. https://doi.org/10.1016/BS.IRCMB.2015.07.006.
56. Wang, Z., Li, Y., Ahmad, A., Banerjee, S., Azmi, A.S., Kong, D., and Sarkar, F.H. (2011). Pancreatic cancer: Understanding and overcoming chemoresistance. Nat Rev Gastroenterol Hepatol *8*, 27–33. https://doi.org/10.1038/nrgastro.2010.188.
57. Khalaileh, A., Dreazen, A., Khatib, A., Apel, R., Swisa, A., Kidess-Bassir, N., Maitra, A., Meyuhas, O., Dor, Y., and Zamir, G. (2013). Phosphorylation of ribosomal protein S6 attenuates DNA damage and tumor suppression during development of pancreatic cancer. Cancer Res *73*, 1811–1820. https://doi.org/10.1158/0008-5472.CAN-12-2014.
58. Tang, Y., Luo, J., Zhou, Y., Zang, H., Yang, Y., Liu, S., Zheng, H., Ma, J., Fan, S., and Wen, Q. (2022). Overexpressed p-S6 associates with lymph node metastasis and predicts poor prognosis in non-small cell lung cancer. BMC Cancer *22*, 564. https://doi.org/10.1186/S12885-022-09664-4.
59. Weidenauer, K., Schmidt, C., Rohde, C., Pauli, C., Blank, M.F., Heid, D., Waclawiczek, A., Corbacioglu, A., Göllner, S., Lotze, M., et al. (2023). The ribosomal protein S6 kinase alpha-1 (RPS6KA1) induces resistance to venetoclax/azacitidine in acute myeloid leukemia. Leukemia *37*, 1611–1625. https://doi.org/10.1038/s41375-023-01951-8.
60. De, A., Jacobson, B.A., Peterson, M.S., Jay-Dixon, J., Kratzke, M.G., Sadiq, A.A., Patel, M.R., and Kratzke, R.A. (2018). 4EGI-1 represses cap-dependent translation and regulates genome-wide translation in malignant pleural mesothelioma. Invest New Drugs *36*, 217–229. https://doi.org/10.1007/s10637-017-0535-z.

FIGURES

Figure 1. Tunneling nanotubes form in 2D cultures of primary PDAC and in PANC-1 cell line treated with gemcitabine. (A) Cells in 2D cultures of fine-needle biopsy samples from a PDAC patient BJPN0015 develop TNTs. (B) PANC-1 cell line increases the number of TNTs in response to gemcitabine. Green, CellMask Green (actin); red, TMRM (mitochondria); blue, Hoechst 33342 (DNA). (C) Linear model of the dose-dependence of TNT formation on gemcitabine concentration. (D) Confocal 3D reconstruction of one TNT between PANC-1 cells with depth coding showing that the TNT is above the substrate. Further images in Supplementary figure S1.

Figure 2. Ribosomal components, mRNA and fully assembled ribosomes detected in tunneling nanotubes. Ribosomal components 5.8S rRNA (A), ribosomal protein S6 (B), ribosomal protein L24 (C), poly-A mRNA (D), complete ribosomes (E) and ribosomal protein S9 (F) found in TNTs formed between PANC-1 cells in culture after a 48-hour exposure to 0.5 μM gemcitabine. 5.8 rRNA (G, J) and complete ribosomes (H, K) detected in TNTs formed between patient-derived cells in culture, accompanied by cytokeratin 19 (I) and vimentin (L). Images from a confocal microscope (*) and from a fluorescent microscope (#). Further images in Supplementary figure S2.

Figure 3. Ribosomal component RPS9 is transported between cells via TNTs and incorporated into ribosomes. HaloTag-labelled RPS9 is transported to untransfected PANC-1 cells labelled with a blue CellTrace™ Violet stain (A) or to PANC-1 cells transfected with nuclear targeted GFP (B). Complete ribosomes detected in TNTs between PANC-1 cells by the RPS9-RPL24 proximity ligation assay (C) or by the HaloTag-RPS9-RPL24 proximity ligation assay, showing the incorporation of the labelled RPS9 into complete ribosomes. Transfected/untransfected PANC-1 cells were mixed in culture and then exposed for 48 hours to 0.5 μM gemcitabine. Images from a confocal microscope (*) and from a fluorescent microscope (#). Further images in Supplementary figure S3.

Video 1. Live cell imaging of HaloTag RPS9 transport in TNTs between PANC-1 cells. A movement of the HaloTag labelled RPS9 within TNTs formed between PANC-1 cells in culture after a 48 hours exposure to 0.5 μM gemcitabine (3.873 seconds per frame).

A Tumor samples form TNTs in 2D culture

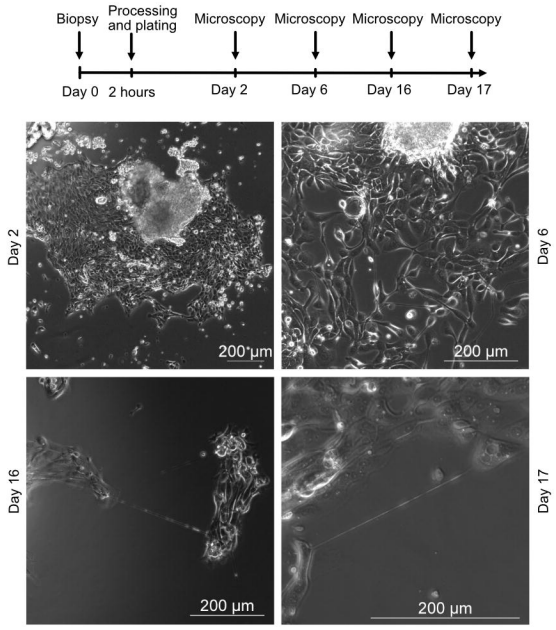

B Gemcitabine induces TNT formation

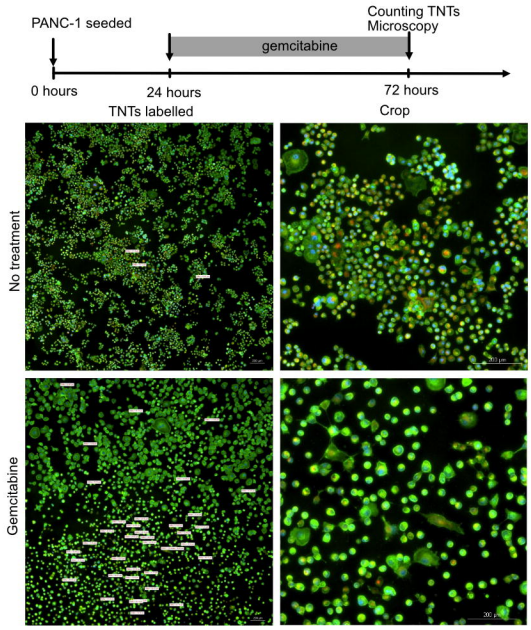

C Gemcitabine induces TNTs in PANC-1

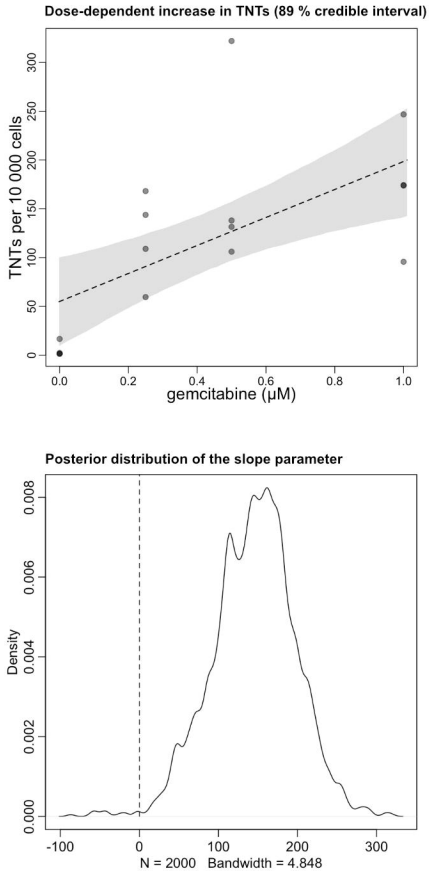

D Depth-coded 3D confocal image of a TNT

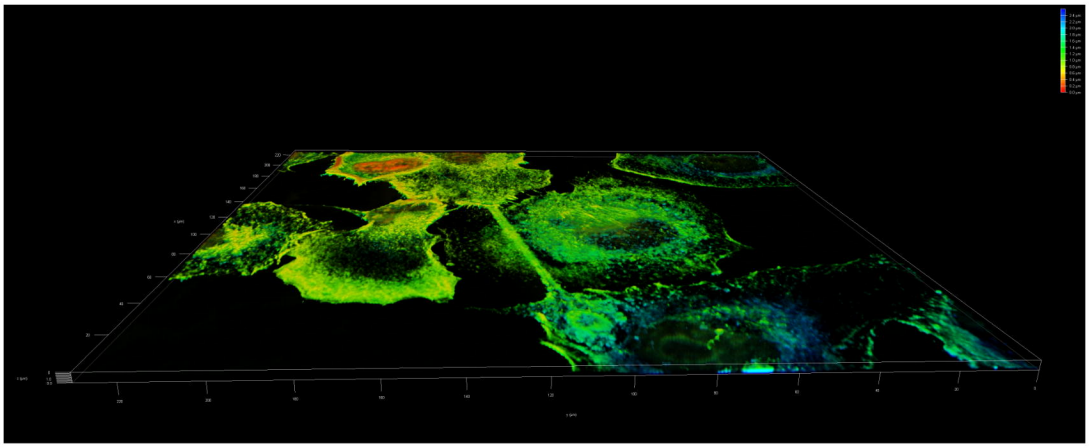

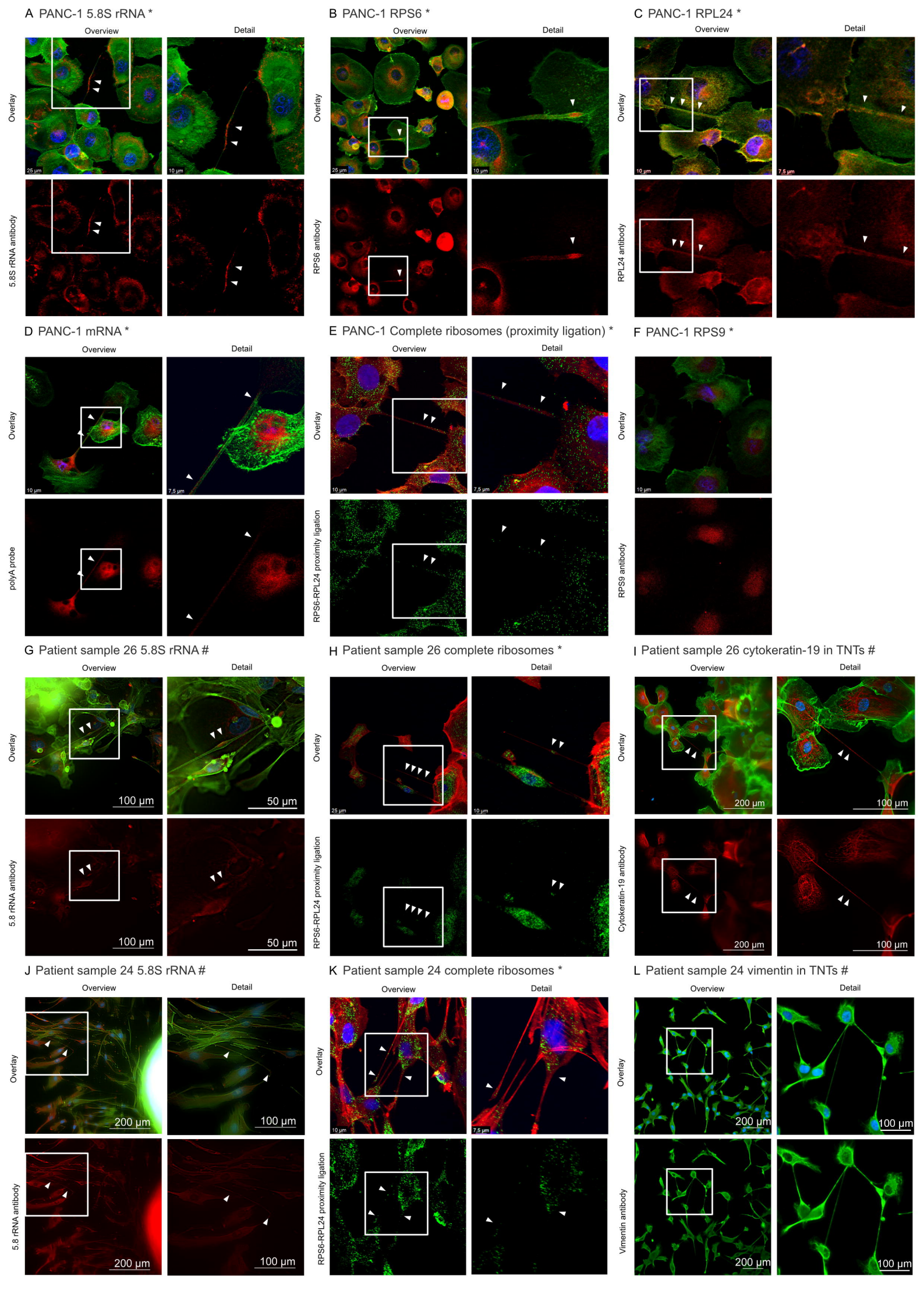
A PANC-1 5.8S rRNA *
B PANC-1 RPS6 *
C PANC-1 RPL24 *
D PANC-1 mRNA *
E PANC-1 Complete ribosomes (proximity ligation) *
F PANC-1 RPS9 *
G Patient sample 26 5.8S rRNA #
H Patient sample 26 complete ribosomes *
I Patient sample 26 cytokeratin-19 in TNTs #
J Patient sample 24 5.8S rRNA #
K Patient sample 24 complete ribosomes *
L Patient sample 24 vimentin in TNTs #
Overview
Detail
Overlay
5.8S rRNA antibody
RPS6 antibody
RPL24 antibody
polyA probe
RPS6-RPL24 proximity ligation
RPS9 antibody
5.8 rRNA antibody
Cytokeratin-19 antibody
Vimentin antibody
25 µm
10 µm
7,5 µm
100 µm
50 µm
200 µm

A Transport of HaloTag RPS9 (red) to untransfected cells (blue) in PANC- 1 #

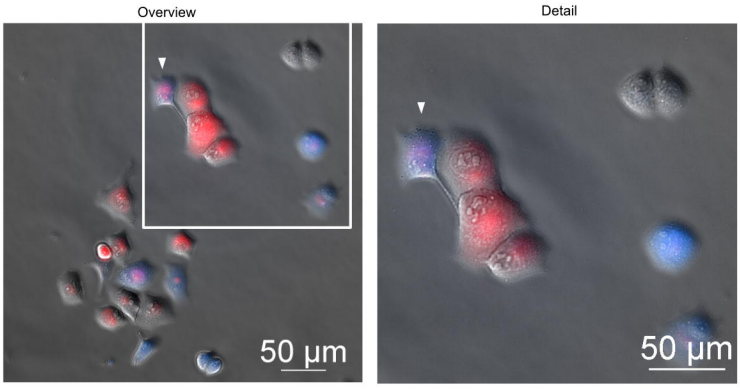

B Transport of HaloTag RPS9 (red) to nuclear GFP cells (green) in PANC- 1 #

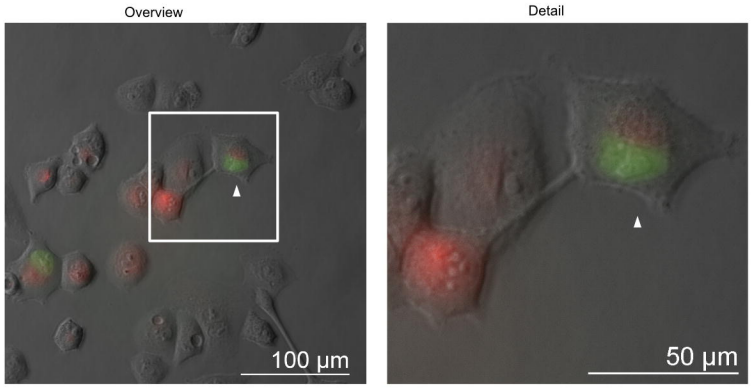

C Proximity ligation assay RPS9-RPL24 in PANC- 1 *

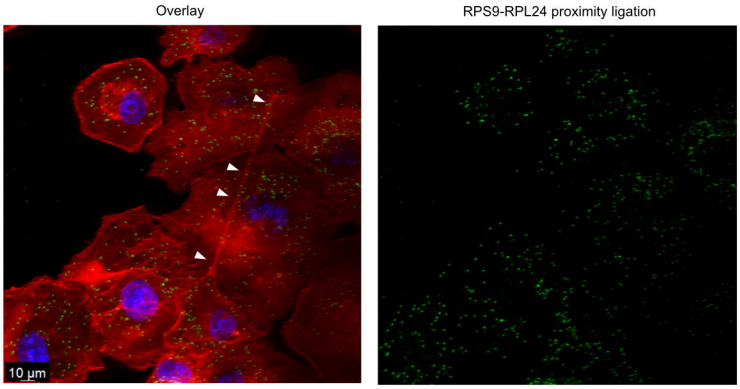
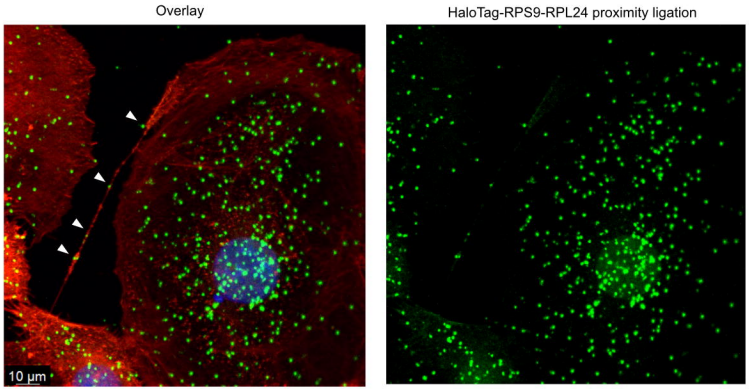
D Incorporation of HaloTag-RPS9 into ribosomes in PANC- 1 *